Kinetic insight into the electrochemical sodium insertion-extraction mechanism of the puckered γ'-V2O5 polymorph

M. Safrany Renard, Rita Baddour-Hadjean, J.-P. Pereira-Ramos

Kinetic insight into the electrochemical sodium insertion-extraction mechanism of the puckered γ'-V_2O_5 polymorph

M. Safrany-Renard, R. Baddour-Hadjean*, J.P. Pereira-Ramos

Institut de Chimie et des Matériaux Paris Est (ICMPE), UMR 7182 CNRS-Université Paris Est Créteil, 2 rue Henri Dunant, 94320 Thiais, France

**corresponding author: baddour@icmpe.cnrs.fr*

Abstract

The kinetics of the electrochemical Na reaction in the γ'-V_2O_5 polymorph prepared by the carboreduction route is investigated by electrochemical impedance spectroscopy. This cathode material with puckered layer structure is capable of delivering a high discharge capacity of 143 mAh g^{-1} at a relatively high operating voltage of 3.3 V vs. Na^+/Na. In spite of a good cyclability, a low efficiency of the first charge process limits yet the value of the stable capacity of this material upon cycling. The present study intends to give further insight into the sodium insertion-extraction mechanism in γ'-V_2O_5 by achieving a picture of the main kinetic parameters as a function of Na uptake in γ-$Na_xV_2O_5$ electrodes ($0 \leq x \leq 0.97$). We show that the evolution of cathode impedance, charge transfer resistance, double layer capacity and apparent chemical Na diffusion coefficient are highly correlated to the structural changes induced upon sodiation. A faster Na diffusion is revealed in the richest $0.6 < x \leq 0.97$ solid solution region while electron transport is slowed down in that composition domain due to the highly localized electron character of the sodiated phase. A significant modification of the surface area is also underlined, undoubtedly caused by the high volume expansion experienced during sodiation. The low efficiency of the first cycle, characterized by an important polarization at the end of the charge, is explained by a huge increase in the electrode impedance.

Keywords: γ'-V_2O_5, cathode material, kinetics, Na diffusion, Na-ion battery

Introduction

Lithium-ion batteries (LIBs) constitute the best energy storage technology for portable equipment, EV and large-scale applications when combined with renewable energies. Intense research toward Na-ion batteries (NIBs) is explained by the too limited lithium reserves in the earth. Furthermore, sodium has similar intercalation chemistry with only a lower reduction voltage of ≈ 0.3 V and greater extent of chemical safety. One of the main challenging problems is the identification of promising cathode materials and a wide variety of compounds has been already screened [1]. Various sodiated oxides were studied as potential cathode materials for NIBs like Na_xCoO_2 [2], $Na_{2/3}(Fe_{0.5}Mn_{0.5})O_2$ [3], $NaMnO_2$ [4], $NaCrO_2$ [5], Na_xVO_2 [6,7], $Na_{1+y}V_3O_8$ [8], $Na_{0.33}V_2O_5$ [9,10]. The lower operating voltage of NIBs results in enhanced stability of the non-aqueous electrolyte, but also leads to lower energy density. Moreover, large distortions detrimental to cycle life occur in the host lattice during sodiation/desodiation process [11]. Layered materials with Van der Waals interlayer spacing appear therefore as ideal host lattices from which limited structural distortions and consequently good cycling behaviour can be expected.

With an open structure allowing the achievement of a high capacity (≈ 300 mAh g^{-1} in the 4 V-2.1 V voltage window), the thermodynamically most stable form of vanadium pentoxide α-V_2O_5 is considered as a model for insertion reactions for rechargeable Li batteries [12]. In spite of its attractive electrochemical properties toward Li insertion, Na insertion into α-V_2O_5 has been addressed only recently [13]. Electrochemical sodiation of α-V_2O_5 leads to the irreversible formation of a genuine NaV_2O_5 bronze capable of delivering a moderate capacity of 80-100 mAh g^{-1} available at 1.8 V vs Na^+/Na at C/5-C/10, respectively.

More recently, we gave evidence in our group for the interest of another metastable polymorph, namely γ'-V_2O_5 as cathode material for LIBs [14,15] and NIBs [14, 16-18]. γ'-V_2O_5 exhibits a layered structure differing from that of α-V_2O_5 by a pronounced layer puckering, composed of infinite ribbons made of VO_5 edges-sharing distorted pyramids with a large interlayer spacing of 5.02 Å (vs. 4.37 Å in α-V_2O_5) [16]. It is worth noting that sodium insertion in γ'-V_2O_5 occurs at a high working voltage of 3.3 V vs Na^+/Na, and remarkably at the same energy level than lithium insertion [14,15]. A high initial discharge capacity of 143 mAh g^{-1} was reported in a sodium cell, followed by a low first charge efficiency (62% at C/20) but excellent capacity retention on further cycling [16]. In the same paper, a detailed structural study has pictured the sodiation mechanism involved in the $0 \leq x \leq 1$ composition range in γ-$Na_xV_2O_5$ [16]. Herein, we report a detailed kinetics investigation of the electrochemical sodiation process involved in

γ'-V_2O_5. The key parameters of the Na insertion-extraction reaction are obtained from an electrochemical impedance study (EIS) as a function of x in γ $Na_xV_2O_5$ ($0 \leq x \leq 0.97$). Their evolution is discussed at the light of the structural mechanism involved in γ'-V_2O_5. The achieved findings allow to get a full understanding of this promising cathode material and opens directions for further optimization of the γ'-V_2O_5 polymorph as efficient positive electrode material for NIB.

Experimental

γ'-V_2O_5 is obtained by chemical oxidation of γ-LiV_2O_5 prepared by the carbothermal reduction method [19]. A topotactic and quantitative lithium removal from the bronze precursor is achieved. The reaction is performed in acetonitrile using NO_2BF_4 (solid Alfa Aesar 96%) as oxidizing agent as described in [15]. After 24h under stirring at room temperature, the obtained powder is washed with acetonitrile several times before drying at 70°C. The powder color changing from black to orange confirms the complete lithium deintercalation. Electrochemical and chemical redox titration confirmed the 5+ oxidation state of vanadium in γ'-V_2O_5. Two-electrode coin cells (CR 2032) with sodium disk as reference and auxiliary electrodes were used to perform electrochemical studies. γ'-V_2O_5 positive electrode was prepared by mixing 80 wt % of active material, 7.5 wt% of acetylene black, 7.5 wt% of graphite and 5wt% of teflon as binder agent. About 8 mg of this mixture was pressed on a stainless steel grid (8 mm diam, 0.35 mm thick) under a pressure of 5 tons per cm^2. The separator consists of three glass Whatman microfiber filters soaked by a solution of 1M $NaClO_4$ in propylene carbonate (PC) as electrolyte with FEC (2% vol.) as additive. All the coin cells were assembled in an argon-filled glove box where water and oxygen concentrations were kept less than 1 ppm. Electrochemical experiments were performed at 20°C using a VMP3 Biologic apparatus.

Impedance measurements were carried out at 20°C in a conventional three-electrode cell under argon atmosphere. The cell was filled with 1M $NaClO_4$ in PC. The positive electrode was made of the same composite electrode as the one used in coin cells. Reference electrode was made of a Li wire placed in a separate compartment filled up with lithiated PC electrolyte to ensure a reliable and stable potential, while a high surface gold wire acted as counter electrode. The working electrode composition was adjusted by coulometric titration using a low current density corresponding to a C/20 rate. Equilibrium was considered to have been reached when the open circuit voltage remained stable (< 0.2 mV for 1h). A discharge curve performed at very low current of 1.5 mA g^{-1} (C/100 rate) constitutes a quasi- OCV curve. Impedance

measurements were performed in the frequency range 10^5 Hz to 0.5 10^{-3} Hz with a VMP3 Biologic Multipotentiostat-Galvanostat apparatus. The geometric surface area of the working electrode dipped in the 3-electrode cell for impedance measurements is 1 cm^2. The excitation signal was 10 mV peak to peak. All these electrochemical measurements were performed in an argon-filled glove box.

Results and discussion

The X-ray diffraction pattern of the γ'-V_2O_5 powder is shown in **Figure 1**. All the diffraction lines can be indexed on the basis of an orthorhombic symmetry (space group *Pnma*) with the following unit cell parameters: a = 9.94 Å; b = 3.58 Å; c = 10.04 Å in good agreement with previous reports [14-16]. The chemical oxidation of γ-LiV_2O_5 obtained by the carbothermal reduction method at 600°C leads to an orange γ'-V_2O_5 powder consisting of big aggregates made of platelets of a few µm (see SEM micrograph of the pristine powder, inset in **Figure 1**). γ'-V_2O_5 is characterized by a high *00l* preferred orientation corresponding to the stacking of platelets along the c axis. This layered structure is composed of infinite ribbons parallel to the b axis made of VO_5 distorted pyramids oriented alternatively up and down. These ribbons are linked together along the a direction to form puckered slabs stacked along the c direction. (see inset in **Figure 2**).

The quasi-OCV curve of γ'-V_2O_5 performed at C/100 rate (**Figure 2**) exhibits one voltage quasi-plateau appearing very early, near 3.3 V vs. Na^+/Na. A stable potential of 3.33 V characterizes the first part of the discharge ($0.02 \leq x \leq 0.5$ in γ-$Na_xV_2O_5$). Then, it decreases slowly to 3.29 V in the second part of the discharge ($0.5 \leq x \leq 0.8$) before dropping abruptly to 1.8 V to reach a maximum sodium uptake of 0.97 Na/V_2O_5 (see inset in **Figure 2**).

A detailed structural study has reported a two-phase region along the first part of the discharge characterized by a voltage plateau, where γ'-V_2O_5 and γ-$Na_{0.7}V_2O_5$ coexist ($0 \leq x < 0.7$), then a solid solution domain for $0.7 \leq x \leq 0.97$ in γ-$Na_xV_2O_5$ [16]. The γ-$Na_xV_2O_5$ phase produced from the first Na content exhibits the following unit cell parameters: a = 9.78 Å; b = 3.61 Å; c = 11.94 Å. As shown in **Figure 3a-b-c**, the lattice parameters of the γ-$Na_xV_2O_5$ phase remain quasi constant in the whole existence domain ($0.05 \leq x \leq 0.97$). The unit cell parameters of the Na-rich γ-$Na_{0.97}V_2O_5$ phase are a = 9.76 Å; b = 3.63 Å; c = 11.94 Å. Hence, sodiation of γ'-

V_2O_5 induces a strong expansion of the interlayer *c* parameter (+19%). Conversely, a slight contraction of the *a* parameter is found (-1.8%) whereas the *b* parameter exhibits a negligible increase (+1.3%). Consequently, a noticeable unit cell volume expansion occurs, from 357 to 420 $Å^3$, i.e. +17% compared to γ'-V_2O_5 (**Figure 3d**).

As shown in **Figure 4**, the first discharge-charge curve of γ'-V_2O_5 performed at C/10 (15 mA g^{-1}) shows one single reduction step at c.a. 3.3 V corresponding to the incorporation of 0.97 Na/V_2O_5 leading to a specific capacity of 143 mAh g^{-1} [16]. An interesting rate capability behavior was reported for γ'-V_2O_5, with still discharge capacities of 140 mAh g^{-1} at C/2, 120 mAh g^{-1} at C and 117 mAh g^{-1} at 2C [16]. However, the charge process is not quantitative as only a 53% charge efficiency is observed at the moderate C/10 rate (**Figure 4**). Examination of the specific capacities and charge efficiencies involved during the first cycle of γ'-V_2O_5 as a function of the C rate (**Table 1**) shows indeed that the rate capability in charge is not as good as in discharge. This behavior is typical of the first cycle, a good capacity retention being reported from the second cycle with still 70 mAh g^{-1} available at C/10 after 70 cycles [16]. Data reported in **Table 1** show also that the charge efficiency increases with decreasing C-rate. This result suggests some important discrepancy in the discharge and charge kinetics and prompted us to examine in details the kinetics of electrochemical sodiation in γ'-V_2O_5 as a function of depth of discharge and charge.

The typical impedance spectra obtained for γ-$Na_xV_2O_5$ electrodes are reported in **Figure 5** (for $0 \leq x \leq 0.6$) **and Figure 6** (for $0.6 < x \leq 0.97$). Two kinds of Nyquist diagrams are observed, depending on the x value. For $0 < x \leq 0.6$, all the spectra gathered in **Figure 5** show a well-defined charge transfer semi-circle centered at 160-400 Hz followed by a straight line with a phase angle of 45° corresponding to the Warburg region (when $\omega >> 2D_{Na}/L^2$, L being the maximum length of the diffusion pathway). This behaviour is in line with that expected for a standard insertion compound [20]. The electrolyte resistance does not exceed 10 Ω. An enlarged view of the high frequency region (**Figure 5b**) points to a continuous increase in the charge transfer semicircle with the sodium content. Indeed, the charge transfer resistance R_{ct} increases from 22 to 39 Ω while at the same time, the characteristic frequency decreases from 400 Hz for x = 0 to 160 Hz for x = 0.6. Finally, the lowest impedance values are found for x = 0.3 and 0.4.

For higher Na contents, i.e. for $0.6 < x \leq 0.97$ (**Figure 6)**, a change in the shape of the diagrams is observed, with a high frequency distorted semi-circle centered at 80 Hz instead of 160-400 Hz for $x \leq 0.6$. These distorted semicircles do not loop on the real axis, indicating the time constants of the different processes are not well separated. It is worth noting a shortening of the Warburg regions followed by well-defined quasi-vertical lines corresponding to the finite diffusion process ($\omega << 2D_{Na}/L^2$). Such a behavior reveals a faster cation diffusion for the richest Na compositions. Finally, the cathode impedance is significantly larger in the last part of the discharge.

The crucial electrochemical parameters of the sodiated electrode such as cathode impedance, charge transfer resistance and double layer capacity are gathered in **Figures 7a, 7b and 7c,** respectively**.** Except for the very low sodium contents characterized by a high cathode impedance, in the order 300-400 Ω, the cathode impedance increases with the sodium uptake from around 100 Ω for x = 0.2 to 350 Ω for x = 0.6 and 700 Ω for x = 0.97 (**Figure 7a**). The cathode impedance of the fully sodiated sample is nearly twice that of sodium-free electrode. This high impedance value is undoubtedly related to the difficult sodium extraction highlighted above (**Figure 4** and **Table 1**).

Simultaneously, the continuous and linear increase in R_{ct} with x (**Figure 7b**) reveals a slowdown of the charge transfer kinetics during the discharge. Indeed, R_{ct} is increasing from 22 to 38 Ω in the biphasic region (where γ'-V_2O_5 and γ-$Na_{0.7}V_2O_5$ coexist) while a much sharpened increase (by a factor 2) is observed in the $0.7 < x \leq 0.97$ solid solution domain. This evolution outlines the detrimental effect of deep sodiation on electron transport. Consequently, the exchange current density linearly decreases with x, from 1 mA cm^{-2} for γ'-V_2O_5 to only 0.4 mA cm^{-2} for γ-$Na_{0.97}V_2O_5$.

The upward trend of the charge transfer resistance suggests that increasing V^{4+}/V^{5+} ratio is detrimental to the electronic conduction. This assumption is supported by the crystallographic data reported for the two types of vanadium environment available in the Na-free γ'-V_2O_5 phase and the fully sodiated γ-$Na_{0.97}V_2O_5$ phase [21]. Indeed, V_aO_5 and V_bO_5 pyramids volumes are similar in γ'-V_2O_5 (4.461 $Å^3$ and 4.531 $Å^3$, respectively), due to the presence of V^{5+} ions in both polyhedra. Conversely, in γ-$Na_{0.97}V_2O_5$, different pyramid volumes of respectively 4.649 $Å^3$ and 5.042 $Å^3$ account for the existence of V^{5+} ions in V_aO_5 pyramids and V^{4+} ions in V_bO_5 pyramids. This highly localized electron character highlighted in γ-$Na_{0.97}V_2O_5$ is well

correlated with the highest cathode impedance and charge transfer resistance values observed for the x = 0.97 composition. In addition, a partial loss of interparticle contact due to important volume change between γ'-V_2O_5 and $Na_{0.97}V_2O_5$ (+17%, see **Figure 3d**) cannot be discarded to explain the increase in the cathode impedance with sodiation.

The evolution of the double layer capacity shown in **Figure 7c** calls also for interesting comments. The C_{dl} parameter is found to increase from ≈ 18 μF cm^{-2} for γ'-V_2O_5 to ≈ 30 μF cm^{-2} for $Na_{0.97}V_2O_5$. It is worth noting this significant 50% C_{dl} increase here evidenced during Na insertion contrasts with the more moderate 15% increase reported upon Li insertion in γ'-V_2O_5 [14]. Such a finding can be explained by sodiation of γ'-V_2O_5 generating a larger volume change than lithiation (+17% vs. +4.4%). Other examples also well illustrate the close relationship between C_{dl} and the volume change induced in the cathode material. For instance, C_{dl} was found to slightly increase by 10% for a volume change of 5% in the case of nanosized V_2O_5 [22] whereas C_{dl} was reported to be constant for the $Cr_{0.11}V_2O_{5.16}$ mixed oxide characterized by a limited volume change that does not exceed 3.5% [23].

The evolution of the Nyquist diagrams during the discharge is illustrated in **Figure 8** through the selection of AC impedance spectra of four Na compositions corresponding to the sodium-poor single phase (x = 0.02), the sodium-rich single phase (x =0.9) and the biphasic region (x =0.3 and 0.6). All the diagrams are well defined with the systematic existence of a Warburg region from which the apparent Na chemical diffusion coefficient D_{Na} has been calculated according to equation (1) [20].

$$A_w = V_M.(dE/dx)_x / F\sqrt{2}\, S\, D_{Na}^{1/2} \qquad \omega >> 2D_{Na}/L^2 \qquad \text{Eq. (1)}$$

A_w is the Warburg prefactor, V_M is the molar volume of the compound (V_M= 53.9 $cm^3.mol^{-1}$), S is the geometric surface area of the electrode (1cm^2), $(dE/dx)_x$ is the slope, at fixed x, of the equilibrium potential composition curve (**Figure 2**).

Actually, Eq. (1) was originally derived for the single-phase electrode. For the two-phase system, it is not a real diffusion coefficient of Na-ion diffusion, but an apparent coefficient, which is determined by the diffusion in the single phase and along or across the two-phase boundary. Usually, the cationic diffusion is limited by the two-phase boundaries inside the particles, so the apparent coefficient should be smaller than that in the single phase.

Comparison of Nyquist diagrams for x =0.9 and x =0.6 suggests a faster sodium diffusion in the Na richest compound. Indeed, unlike the x = 0.9 composition, the sodiated electrode for x = 0.6 exhibits a wide Warburg region without any capacitive line. In addition, a high limiting frequency value is found for x = 0.9 (21 mHz), i.e. 2-3 fold higher than that observed for x = 0.02 and x = 0.3. According to the relation $f^*_L \approx D_{Na}/L^2$ [20], this finding indicates a faster kinetics of sodium transport for x = 0.9.

Figure 9 displays the evolution of the apparent chemical diffusion coefficient of sodium ions D_{Na} as a function of x in γ-$Na_xV_2O_5$ ($0 \leq x \leq 0.97$). The rate of sodium transport is very low at the beginning of the sodiation process, then it significantly increases from $\approx 10^{-13}$ cm^2 s^{-1} for x = 0.1 to 10^{-11} cm^2 s^{-1} for x = 0.4. Then, the mid discharge is again characterized by a slowdown in Na diffusion (D_{Na} around 3 10^{-13} cm^2 s^{-1}) while the sodium rich samples (x = 0.8; 0.9; 0.97) exhibit a significantly faster Na transport kinetics by more than one order of magnitude. It is worth noting that the kinetics of sodium transport is faster in the solid solution domain ($x > 0.7$) than in the diphasic region ($x < 0.7$), due to sodium ions overcoming the interphase boundary. The two-phase region of a well-known cathode material of LIBs such as $LiFePO_4$ is also characterized by an apparent chemical Li diffusion coefficient much lower by several orders of magnitude than in Li-rich and Li-poor single-phase regions [24-27]. This finding indicates the diffusion rate is not impacted by increasing Na amount, which is in line with the good rate capability observed for the reduction process [16]. Then, the low charge efficiency (**Figure 4)** would rather be due to the kinetics of charge transfer and high cathode impedance than to a limitation in the rate of Na diffusion. Scarce data are available on Na^+ mobility in sodiated oxides with very close values in the range 10^{-12}-10^{-10} cm^2 s^{-1} reported for instance in $Na_{0.33}V_2O_5$ [28,29], in Na_xCoO_2 [30] and P2-$Na_{0.67}MnO_2$ [31].

In order to understand the origin of the partial extraction of sodium ions from γ-$Na_{0.97}V_2O_5$ (**Figure 4**), we have examined the kinetics features of the charge process. The Nyquist diagrams for various charged γ-$Na_xV_2O_5$ electrodes (x = 0.9, 0.8, 0.7, 0.6 and 0.5) are shown in **Figure 10**. The impedance diagrams significantly differ from the usual shape observed during discharge. The deeper the depth of charge, the more distorted the semicircle and the higher the impedance value. In contrast to what happens during sodiation, the semicircle never joins the real axis, indicating an overlap in time constants of the different phenomena. From the very first extracted sodium ions, the electrode impedance sharply decreases, from 720 to 160 Ω when

x varies from 0.97 to 0.9. Then, the electrode impedance rapidly increases upon charging to reach 130, 260, 420 Ω for x = 0.8, 0.7, 0.6, respectively and finally 840 Ω for x = 0.5. In addition, the R_{ct} value, around 70 Ω, does not change and is about twice that observed throughout sodiation. This evolution indicates a slower kinetics of charge transfer during the charge compared to the discharge process.

The origin of the electrode impedance increase upon charge is not straightforward. However, SEM micrographs (**Figure 11**) reveal a decrease in particle size by a factor 3 after charge, from 10 µm to 2-3 µm. Also, the C_{dl} parameter value does not significantly change and its value at the end of the charge (70 µF cm^{-1}) is twice that observed at the end of the discharge. Both observations indicate a significant modification in electroactive surface area with the emergence of cracks after the charge process that may be responsible for a loss of contact between particles and/or a modification of grain boundaries properties. Such phenomenon would explain the impedance increase during the charge. This trend, combined with a higher charge transfer resistance, has a detrimental effect on the electrochemical kinetics of Na extraction from γ-$Na_{0.97}V_2O_5$ and probably accounts for the poor rate capability observed for the charge reaction.

Conclusion

In this work, we report the kinetics of electrochemical sodium insertion into the γ'-V_2O_5 polymorph cathode material for NIBs, showing reversible sodiation at an appealing high potential of 3.3V vs Na^+/Na. A detailed EIS study has revealed a strong influence of the depth of discharge and charge on the kinetics parameters. During the discharge, the cathode impedance increases to be maximum for the fully sodiated compound γ-$Na_{0.97}V_2O_5$. At the same time, the double layer capacity C_{dl} and charge transfer resistance R_{ct} progressively increase with the sodium content. The great C_{dl} increase by 50% originates from the significant volume expansion occurring on sodiation (+17%). We show the evolution of this parameter is directly linked to the amplitude of the structure changes induced by the Li/Na insertion in γ'-V_2O_5. Indeed, a 15% C_{dl} increase was reported for the lithiated analogue, in line with a lower volume expansion (ΔV/V = 4.4%) [14]. On the other hand, the evolution of the R_{ct} parameter indicates a linear decrease in the charge transfer kinetics with Na content due to the highly localized electron character in the sodiated γ-$Na_xV_2O_5$ phase. The apparent chemical sodium diffusion

coefficient has been calculated as a function of x in γ-$Na_xV_2O_5$ and is found to be the highest in the richest $0.6 < x \leq 0.97$ composition range corresponding to the single-phase region. The kinetics study performed during the charge reveals more distorted impedance diagrams with a fast and significant impedance increase on progressive desodiation. A huge value of 840 Ω is reached at mid-charge, which is responsible for the hysteresis between charging and discharging. This impedes the second part of the charge to be performed and probably explains the low charge efficiency. Moreover, the higher charge transfer resistance also harms the charge efficiency. Great performance improvement toward a quantitative Na extraction upon charge can then be expected from a preliminary ball-milling process of the active material in order to better accommodate the significant volume changes. This work is in progress in our group. In parallel, the development of solution techniques using soft chemistry route is carried out to obtain fine, homogeneous and porous particles with improved performance.

References

[1] N. Yabuuchi, K. Kubota, M. Dahbi, S. Komaba, Research developments on sodium-ion batteries, Chem. Rev. 114 (2014) 11636–11682.

[2] R. Berthelot, D. Carlier, C. Delmas, Electrochemical Investigation of the P2–Na_xCoO_2 Phase Diagram, Nat. Mater. 10 (2011) 74-80.

[3] N. Yabuuchi, M. Kajiyama, J. Iwatate, H. Nishikawa, S. Hitomi, R. Okuyama, R. Usui, Y. Yamada, S. Komaba, V. P2-type $Na_x[Fe_{1/2}Mn_{1/2}]O_2$ made from earth-abundant elements for rechargeable Na batteries, Nat. Mater. 11 (2012) 512-517.

[4] X. Ma, H. Chen, G. Ceder, G., Electrochemical properties of monoclinic $NaMnO_2$, J. Electrochem. Soc. 158 (2011) A1307-1312.

[5] S. Komaba, C. Takei, T. Nakayama, A. Ogata, N. Yabuuchi, Electrochemical intercalation activity of layered $NaCrO_2$ vs. $LiCrO_2$, Electrochem. Commun. 12 (2010) 355-358.

[6] M. Guignard, C. Didier, J. Darriet, P. Bordet, E. Elkaim, C. Delmas, P2-Na_xVO_2 system as electrodes for batteries and electron-correlated materials, Nat. Mater. 12 (2013) 74-80.

[7] D. Hamani, M. Ati, J. M.Tarascon, P. Rozier, Na_xVO_2 as possible electrode for Na-ion batteries, Electrochem. Comm. 13 (2011) 938-941.

[8] G. Venkatesh, V. Pralong, O. I. Lebedev, V. Caignaert, P. Bazin, B. Raveau, Amorphous sodium vanadate $Na_{1.5+y}VO_3$, a promising matrix for reversible sodium intercalation, Electrochem. Comm. 40 (2014) 100-102.

[9] S. Bach, N. Baffier, J. P. Pereira-Ramos, R. Messina, Electrochemical sodium intercalation in $Na_{0.33}V_2O_5$ bronze synthesized by a sol-gel process, Solid State Ion. 37 (1989) 41-49.

[10] H. M. Liu, H. S. Zhou, L. P. Chen, Z. F. Tang, W. S. Yang, Electrochemical insertion/deinsertion of sodium on NaV_6O_{15} nanorods as cathode material of rechargeable sodium-based batteries, J. Power Sources 196 (2011) 814-819.

[11] X. Xiang, K. Zhang, J. Chen, Recent advances and prospects of cathode materials for sodium-ion batteries, Adv. Mater. 27 (2015) 5343-5364

[12] M.S. Whitthingham, Lithium batteries and cathodes, Chem. Rev. 104 (2004) 4271–4301

[13] D. Muller, R. Baddour-Hadjean, M. Tanabe, L. T. N. Huynh, L. M. P. Le, J. P. Pereira-Ramos, Electrochemically formed α'-NaV_2O_5: a new sodium intercalation compound, Electrochim. Acta 176 (2015) 586-593.

[14] M. Safrany Renard, Propriétés électrochimiques et réponse structurale du polymorphe γ'-V_2O_5 vis-à-vis de l'insertion du lithium et du sodium. Paris-East University thesis, 2017. Français. ⟨NNT : 2017PESC1185⟩.

[15] R. Baddour-Hadjean, M. Safrany Renard, J.P. Pereira-Ramos, Unraveling the strucrural mechanism of Li insertion in γ'-V_2O_5 and its effect on cycling properties, Acta Mater. 165 (2019) 183-191.

[16] M. Safrany Renard, N. Emery, R. Baddour-Hadjean, J.P. Pereira-Ramos, γ'-V_2O_5: A new high voltage cathode material for sodium-ion battery, Electrochim. Acta 252C (2017) 4-11.

[17] M. Safrany Renard, N. Emery, E. M. Roginskii, R. Baddour-Hadjean, J. P. Pereira-Ramos, Crystal structure determination of a new sodium vanadium bronze electrochemically formed , J. Solid State Chem. 254 (2017) 62-68.

[18] R. Baddour-Hadjean, M. Safrany Renard, N. Emery, L. T. N. Huynh, M. L. P. Le, J. P. Pereira-Ramos, The richness of V_2O_5 polymorphs as superior cathode materials for sodium insertion , Electrochim. Acta 270 (2018) 129-137.

[19] J. Barker, M. Y. Saidi, J. L. Swoyer, Performance evaluation of the electroactive material γ-LiV_2O_5 made by a carbothermal reduction method, J. Electrochem. Soc. 150 (2003) A1267-A1272.

[20] C. Ho, I. D. Raistrick, R.A. Huggins, Application of AC techniques to the study of lithium diffusion in tungsten trioxide thin films, J. Electrochem. Soc., 127 (1980) 343-350

[21] N. Emery, R. Baddour-Hadjean, D. Batyrbekuly, B. Laïk, Z. Bakenov, J-P. Pereira-Ramos, γ-$Na_{0.96}V_2O_5$: a new competitive cathode material for sodium ion battery synthesized by a soft chemistry route, Chem. Mater. 30 (2018) 5305−5314.

[22] D. Huo, B. Laïk, P. Bonnet, K. Guérin, R. Baddour-Hadjean, J. P. Pereira-Ramos, Electrochemical kinetics of Li insertion in nanosized V_2O_5 high performance obtained via fluorine chemistry, Electrochim. Acta 253 (2017) 472-478.

[23] J. P. Pereira-Ramos, P. Soudan, R. Baddour-Hadjean, S. Bach, A kinetic study of Li transport in the sol-gel $Cr_{0.11}V_2O_{5.16}$ mixed oxide, Electrochim. Acta 56 (2011) 1381-1386.

[24] D. Li, T. Zhang, X. Liu, P. He, R. Peng, M. Wang, M. Han, H. Zhou, A hybrid phase-transition model of olivine $LiFePO_4$ for the charge and discharge processes, J. Power Sources 233 (2013) 299-303.

[25] C. Gao, J. Zhou, G. Liu, L. Wang, Lithium-ions diffusion kinetics in $LiFePO_4$/carbon nanoparticles synthesized by microwave plasma chemical vapor deposition for lithium-ion batteries, Appl. Surf. Sci. 433 (2018) 35-44.

[26] P. P. Prosini, M. Lisi, D. Zane, M. Pasquali, Determination of the chemical diffusion coefficient of lithium in $LiFePO_4$, Solid State Ion. 148 (2002) 45-51.

[27] A. Milev, L. George, S. Khan, P. Selvam, G. S. K. Kannangara, Li-ion kinetics in $LiFePO_4$/carbon nanocomposite prepared by a two-step process: the role of phase composition, Electrochim. Acta 209 (2016) 565-573.

[28] S. Bach, N. Baffier, J. P. Pereira-Ramos, R. Messina, Electrochemical sodium intercalation in $Na_{0.33}V_2O_5$ bronze synthesized by a sol-gel process, Solid State Ion. 37 (1989) 41-49.

[29] D. Jiang, H. Wang, G. Li, G. Li, X. Lan, M. H. Abib, Z. Zhang, Y. Jiang, Self-combustion synthesis and ion diffusion performance of NaV_6O_{15} nanoplates as cathode materials for sodium-ion batteries, J. Electrochem. Soc., 162 (2015) A697-A703.

[30] B. V. R. Reddy, R. Ravikumar, C. Nithya, S. Gopukumar, High performance Na_xCoO_2 as a cathode material for rechargeable sodium batteries, J. Mater. Chem. 3 (2015) 18059-18063.

[31] D. Tie, G. Gao, F. Xia, R. Yue, Q. Wang, R. Qi, B. Wang, Y. Zhao, Modulating the interlayer spacing and Na^+/vacancy disordering of P2-$Na_{0.67}MnO_2$ for fast diffusion and high-rate sodium storage, ACS Appl. Mater. Interf. 11 (2019) 6978-6985.

Figure captions

Figure 1. X-ray diffraction pattern of γ'-V_2O_5. Inset: SEM micrograph of the pristine γ'-V_2O_5 powder

Figure 2. Enlarged view in the 3.5 – 2.5 V region of the quasi-OCV curve of γ'-V_2O_5 performed at 1.5 mA g^{-1} (C/100 rate). Electrolyte 1M $NaClO_4$/PC. Insets: Complete view of the quasi-OCV curve in the 3.5 - 1.8 V voltage window and crystal structure of γ'-V_2O_5.

Figure 3. Evolution of the unit cell parameters unit cell parameters (a-b-c) and volume (d) of the phases formed during the first discharge-charge cycle of γ'-V_2O_5 in 1M $NaClO_4$/PC electrolyte.

Figure 4. First discharge-charge curve of γ'-V_2O_5. Electrolyte 1M $NaClO_4$/PC. C/10 rate.

Figure 5. AC impedance diagrams for γ-$Na_xV_2O_5$ electrodes, $0 \leq x \leq 0.6$ (a); enlarged view of the high frequency region (b).

Figure 6. AC impedance diagrams for γ-$Na_xV_2O_5$ electrodes, $0.6 < x \leq 0.97$.

Figure 7. Evolution of the cathode impedance $|Z|$ (a), charge transfer resistance R_{ct} (b) and double layer capacity C_{dl} (c) in γ-$Na_xV_2O_5$ ($0 \leq x \leq 0.97$).

Figure 8. AC impedance diagrams for γ-$Na_xV_2O_5$ electrodes: x = 0.02; 0.3; 0.6; 0.9

Figure 9. Evolution of the apparent chemical diffusion coefficient of sodium D_{Na} as a function of x in γ-$Na_xV_2O_5$.

Figure 10. AC impedance diagrams for charged γ-$Na_xV_2O_5$ electrodes: x = 0.9; 0.8; 0.7; 0.6; 0.5

Figure 11. SEM micrographs of the initial electrode (a) and electrode after the first discharge-charge cycle at C/10 (b).

TABLES

C rate	C/60	C/20	C/10	C/5	C/2
Discharge capacity	146	143	143	141	140
Charge capacity	112	89	76	65	58
Charge efficiency (%)	77	62	53	46	41

Table 1. Specific capacities (in mAh g^{-1}) and charge efficiency (in %) of the first cycle of a γ'-V_2O_5 electrode in 1M $NaClO_4$ / PC. Voltage window 1.75 - 4 V.

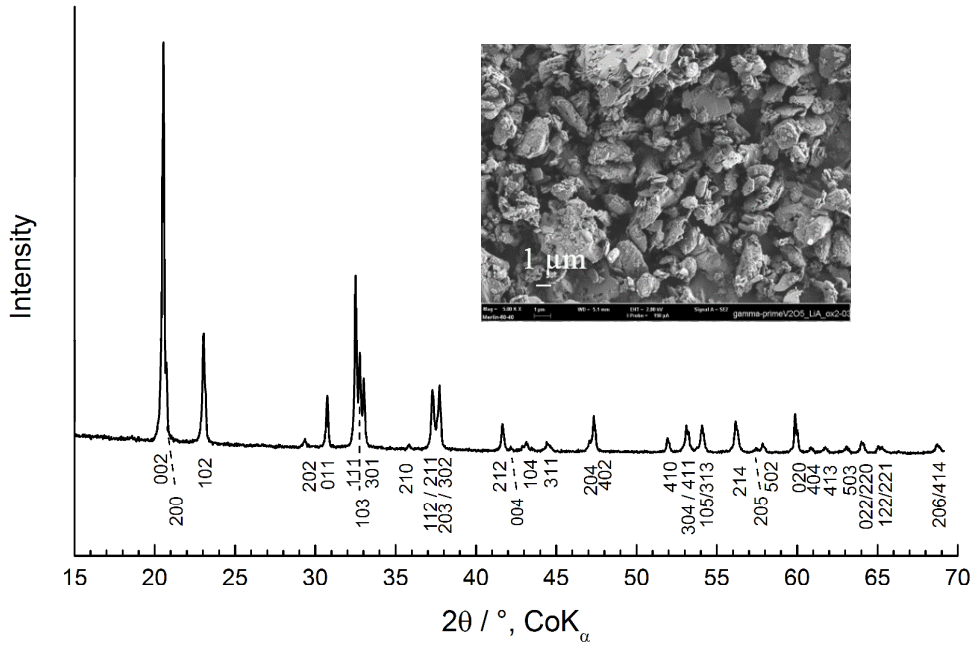

Figure 1. X-ray diffraction pattern of γ'-V_2O_5. Inset: SEM micrograph of the pristine γ'-V_2O_5 powder

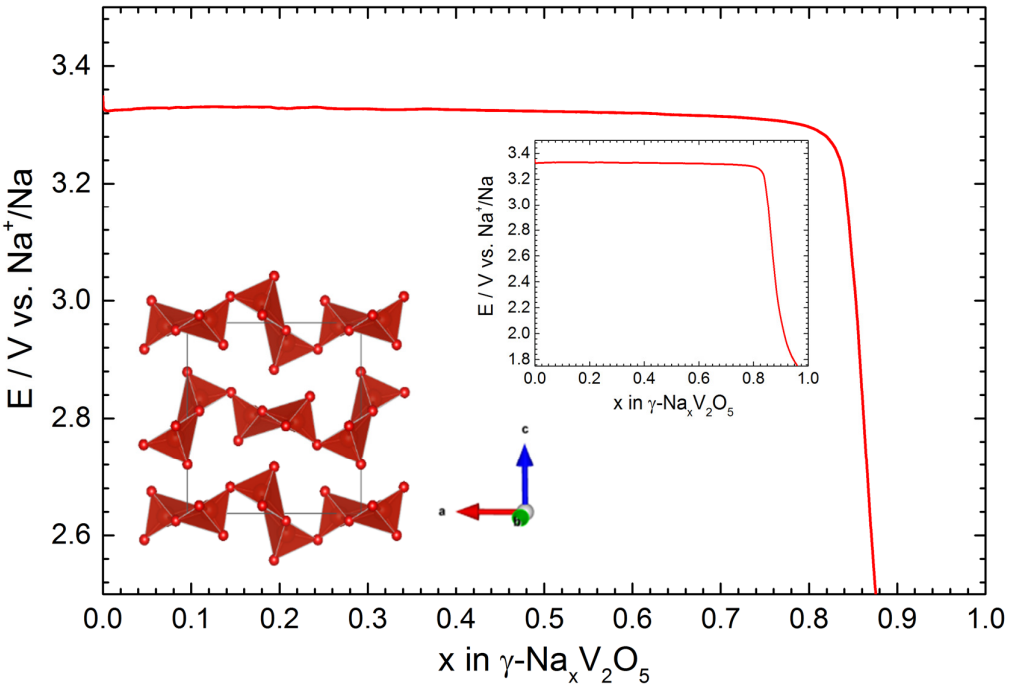

Figure 2. Enlarged view in the 3.5 – 2.5 V region of the quasi-OCV curve of γ'-V_2O_5 performed at 1.5 mA g^{-1} (C/100 rate). Electrolyte 1M $NaClO_4$ /PC. Insets: Complete view of the quasi-OCV curve in the 3.5 - 1.8 V voltage window and crystal structure of γ'-V_2O_5.

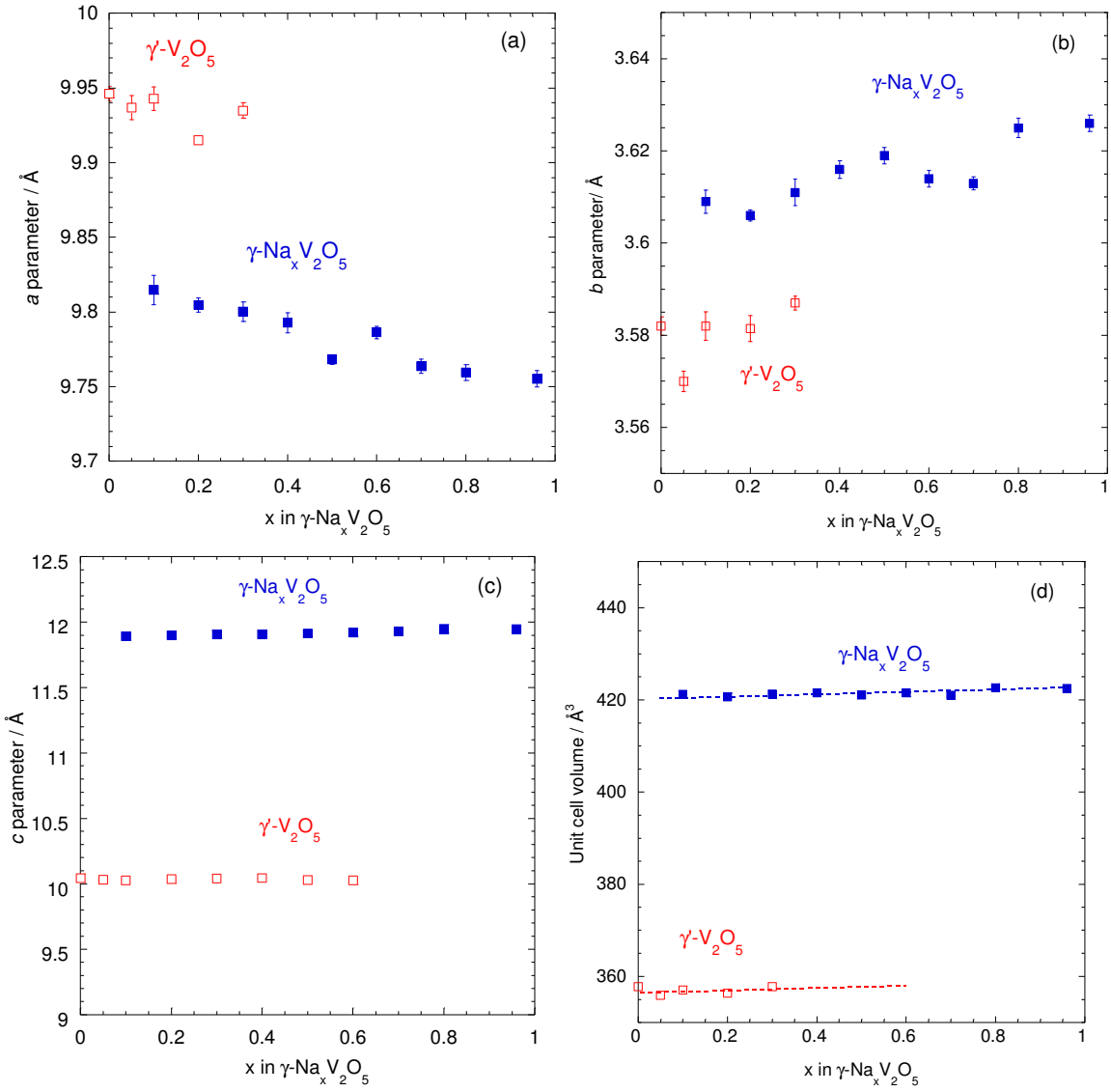

Figure 3. Evolution of the unit cell parameters (a-b-c) and volume (d) of the phases formed during the first discharge-charge cycle of γ'-V_2O_5 in 1M $NaClO_4$/PC electrolyte.

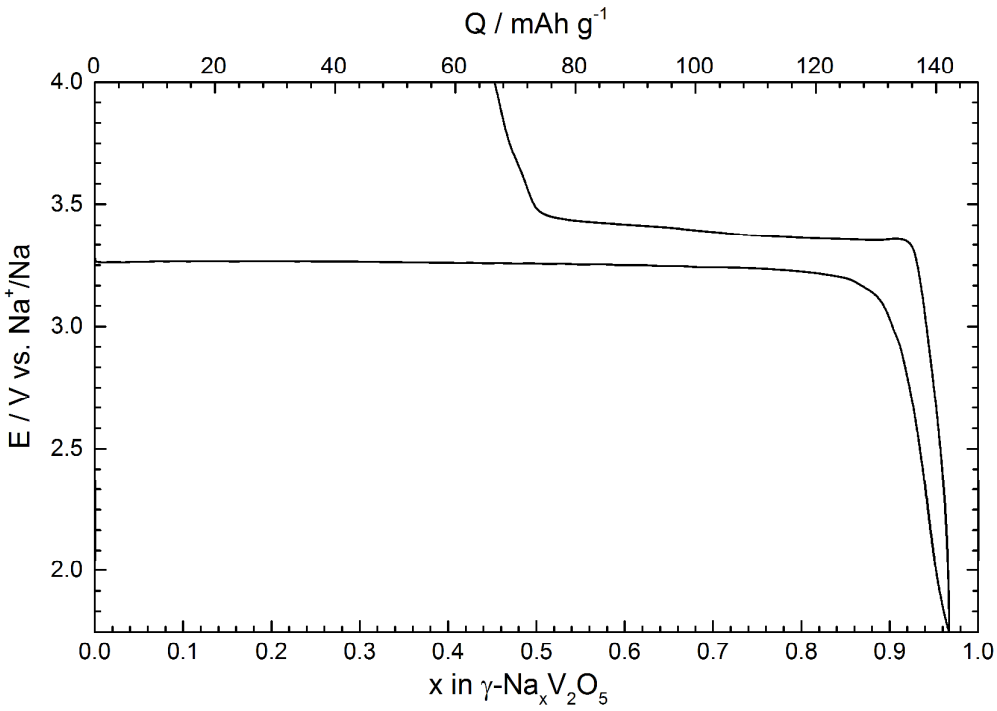

Figure 4. First discharge-charge of γ'-V_2O_5. Electrolyte 1M $NaClO_4$ /PC. C/10 rate.

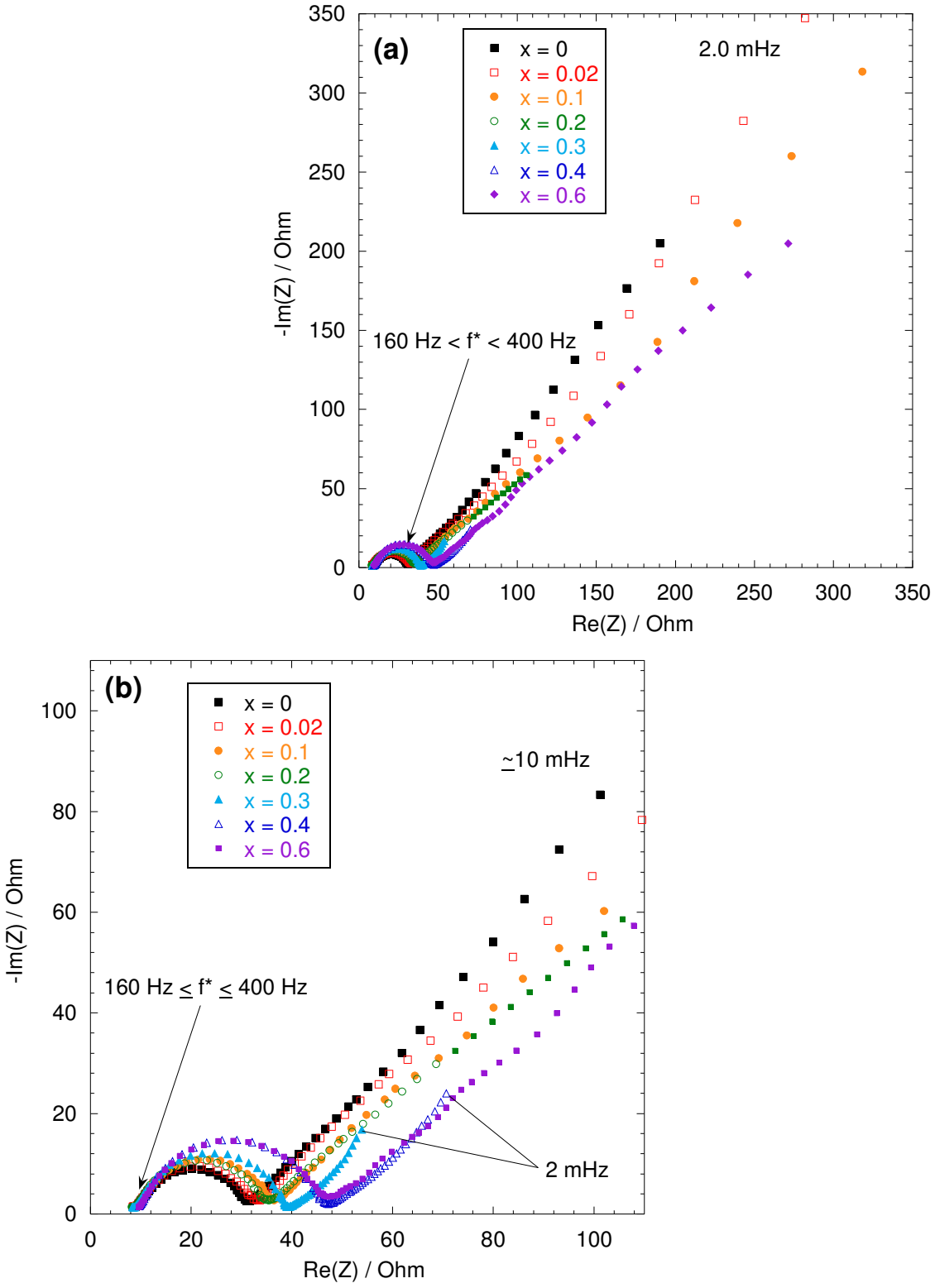

Figure 5. AC impedance diagrams for γ-$Na_xV_2O_5$ electrodes, $0 \leq x \leq 0.6$ (a); enlarged view of the high frequency region (b).

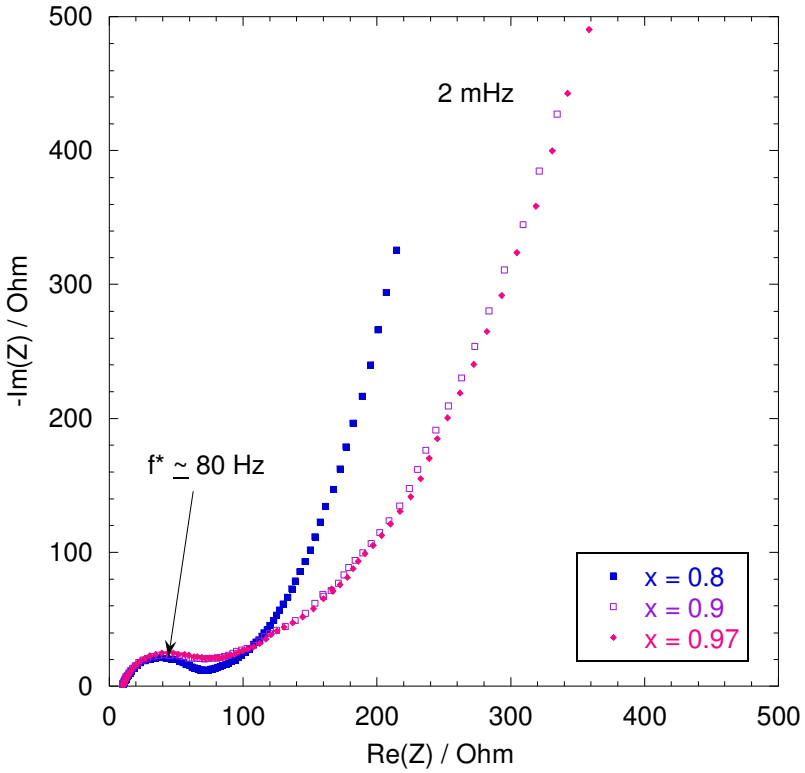

Figure 6. AC impedance diagrams for γ-$Na_xV_2O_5$ electrodes, $0.6 < x \leq 0.97$.

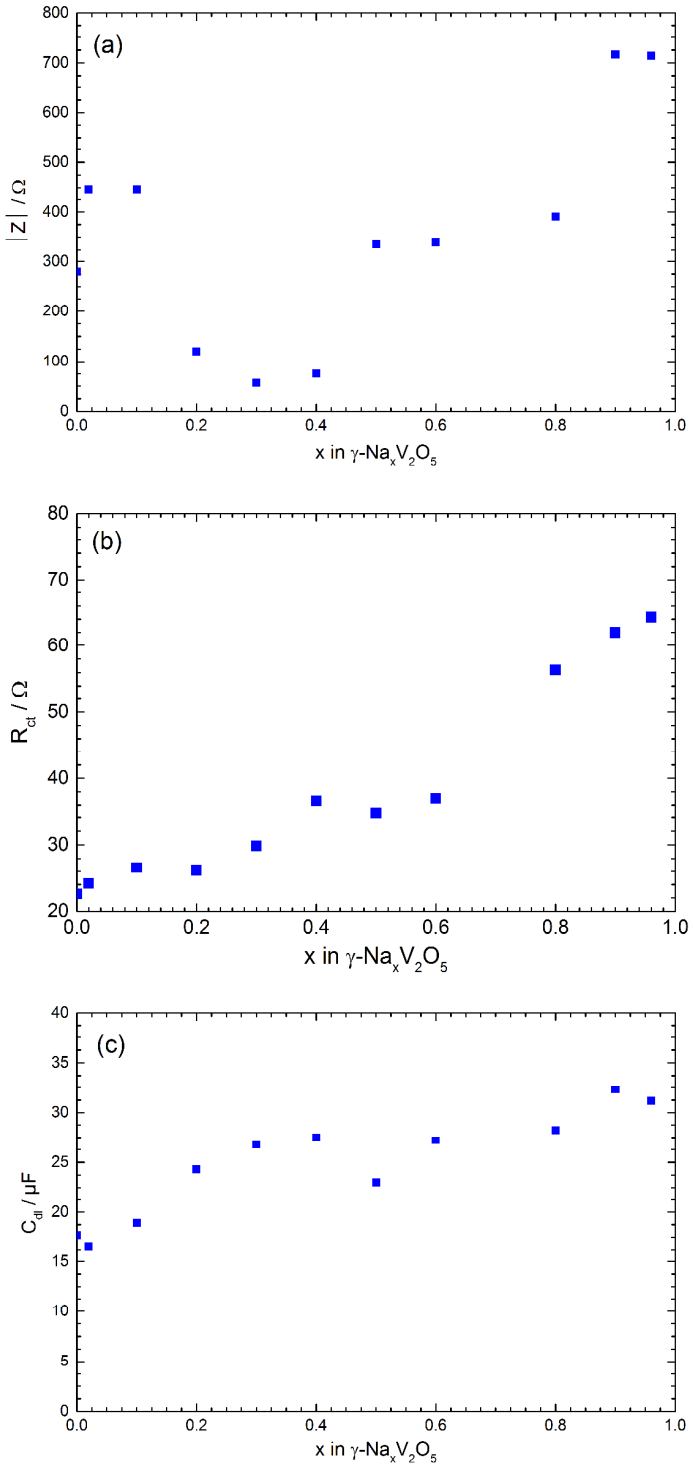

Figure 7. Evolution of the cathode impedance $|Z|$ (a), charge transfer resistance R_{ct} (b) and double layer capacity C_{dl} (c) in γ-$Na_xV_2O_5$ ($0 \leq x \leq 0.97$).

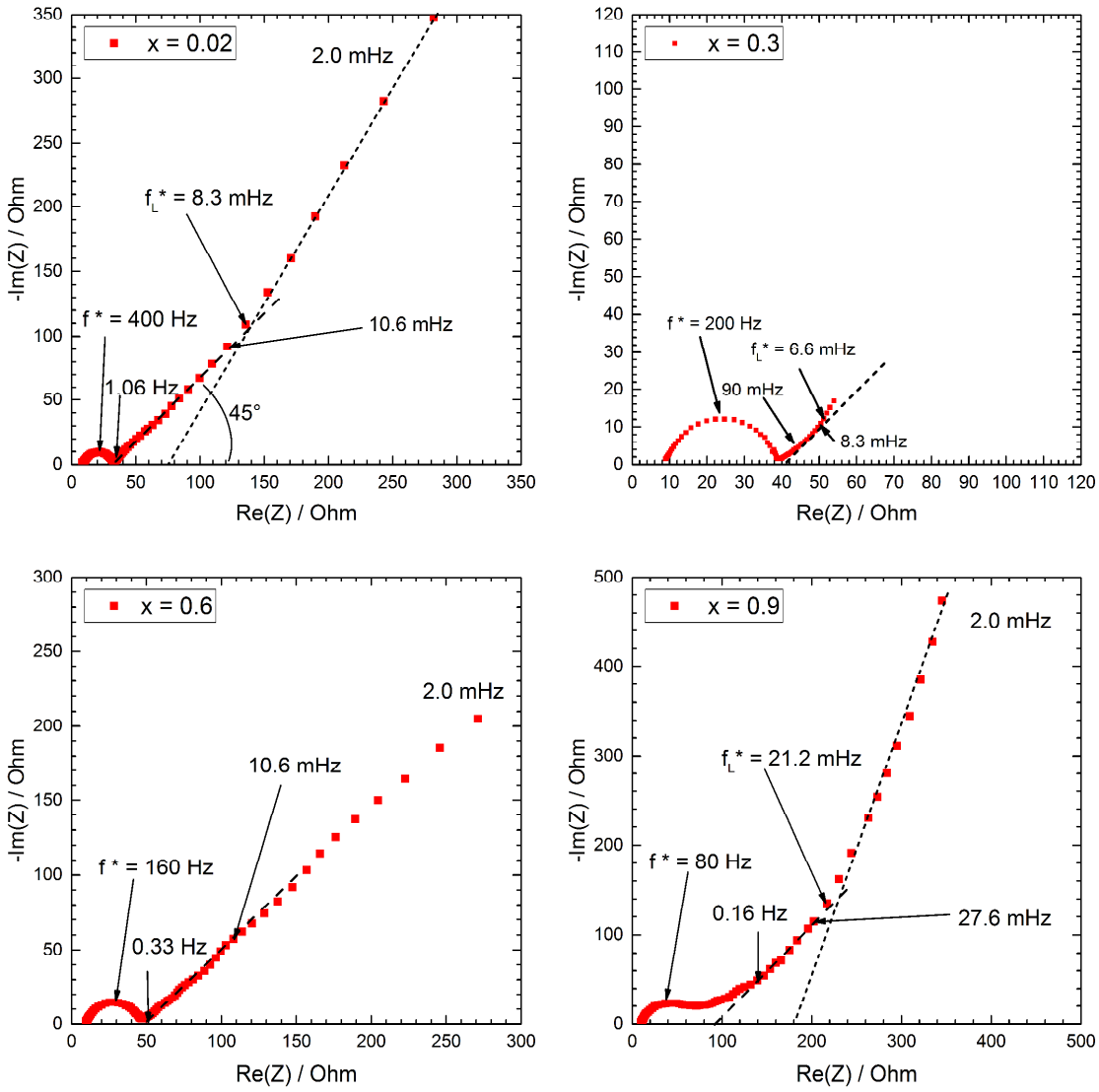

Figure 8. AC impedance diagrams for γ-$Na_xV_2O_5$ electrodes: x = 0.02; 0.3; 0.6; 0.9

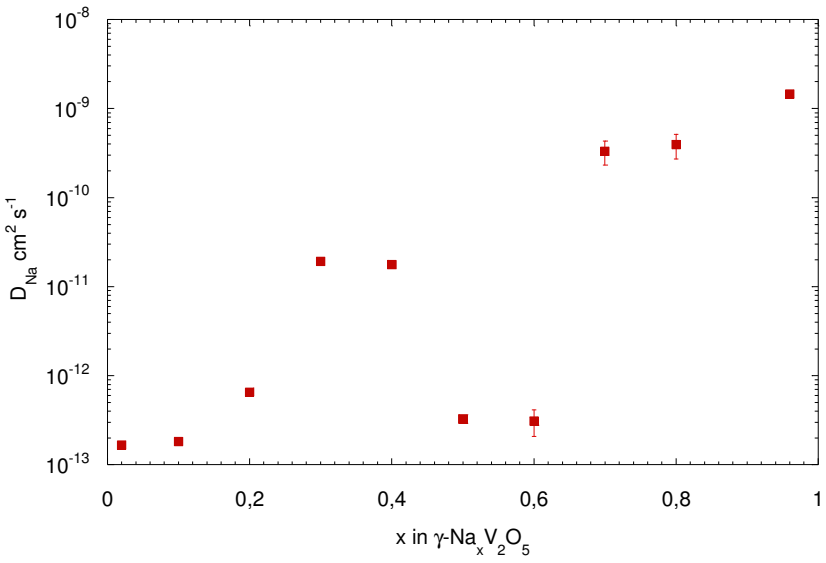

Figure 9. Evolution of the apparent chemical diffusion coefficient of sodium D_{Na} as a function of x in γ-$Na_xV_2O_5$.

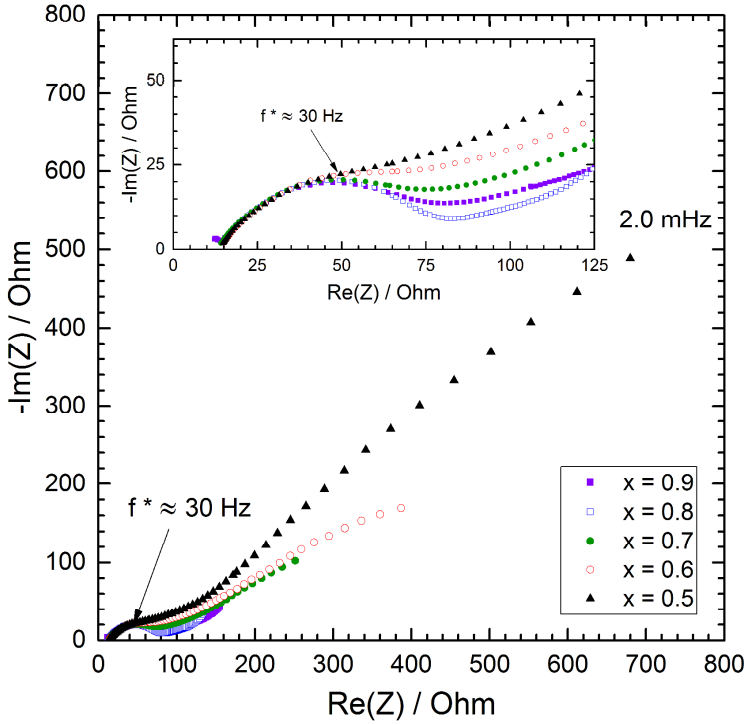

Figure 10. AC impedance diagrams for charged γ-$Na_xV_2O_5$ electrodes: x = 0.9; 0.8; 0.7; 0.6; 0.5

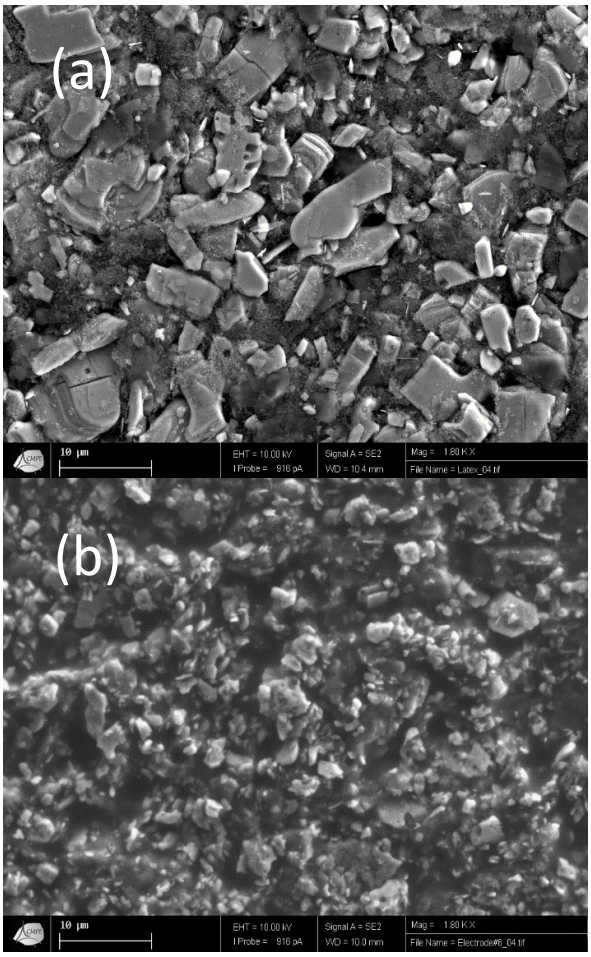

Figure 11. SEM micrographs of the initial electrode (a) and electrode after the first discharge-charge cycle at C/10 (b).